

# Photothermal displacement detection and transient imaging of bump growth dynamics in laser zone texturing of Ni–P disk substrates

Shaochen Chen and Costas P. Grigoropoulos<sup>a)</sup>

*Department of Mechanical Engineering, University of California, Berkeley, California 94720-1740*

Hee K. Park and Pieter Kerstens

*IBM Manufacturing Technology Center, 1798 N. W. 40<sup>th</sup> St., Boca Raton, Florida 33431*

Andrew C. Tam

*IBM Almaden Research Center, 650 Harry Road, San Jose, California 95120*

A novel photothermal displacement method has been applied to probe the pulsed laser-induced feature formation of Ni–P hard disk substrates in the laser zone texturing process. The deflection signals of the reflected probing beam show the variation of the feature shape resulting from different pulse energies of the heating laser beam. A laser flash photography system is also developed to visualize the feature growth dynamics. This system has nanosecond time resolution and about one micron spatial resolution. Both techniques show clearly the transient melting and deformation process and the time scale of such deformation. © 1999 American Institute of Physics.

[S0021-8979(99)32308-2]

## I. INTRODUCTION

Laser-assisted melting and surface modification processes are important in a variety of industrial applications. A well proven technology to improve the stiction performance of hard disk drives for low-flying-height media is the laser zone texturing (LZT) of Ni–P hard disk substrates.<sup>1–3</sup> Many efforts have been contributed to develop different features (“bumps”) and investigate their performance.<sup>3,4</sup> The mechanism of bump formation was also studied by numerical simulation.<sup>5</sup> It was found that the variation of substrate material, laser energy, or substrate surface preparation procedure would significantly affect the laser texture quality (bump shape and bump height).<sup>4,6</sup> However, all these studies were based on the final topography. To well understand the mechanism of bump formation in the LZT process, time and space-resolved investigations are necessary.

Optical heating of solids generates transient displacement of the heated surface that could result in permanent buckling and deformation. Photothermal displacement (PTD) techniques have been developed to measure such displacements by using a probing beam to determine the optical and thermal properties of the sample.<sup>7</sup> However, conventional PTD schemes require high frequency modulation of the heating beam in order to detect a minute deflection signal due to small temperature change or small deformation on the sample surface in the thermoelastic regime.<sup>8,9</sup> In the LZT process, the surface is permanently deformed due to melting after a single pulse heating. The bump diameter is usually from 5 to 20  $\mu\text{m}$  and the height is in the tens of nanometers range respectively. Moreover, conventional PTD setups are not technically practical to monitor the LZT process with the required stability and alignment reproducibility. Recently, a novel PTD setup has been developed to study the transient melting and surface deformation of materials upon single

pulsed-laser heating.<sup>10</sup> This setup provides a robust and high-resolution tool for measuring transient deformation on the material surface. It has the capability of scanning the bump area, of distinguishing the bump shape change due to the heating beam energy variation, and of monitoring the bump height variation in the nanometer range.

Laser flash photography (LFP) has been an efficient tool to study the transient process of laser materials interaction, such as pulsed laser ablation of absorbing liquid,<sup>11,12</sup> laser ablation of solid thin film.<sup>13</sup> One advantage of this technique is that the transient growth process of the whole bump can be visualized.

In this article, results of transient melting and surface deformation from PTD measurement and imaging of transient bump growth dynamics during pulsed laser heating will be presented. Such transient detection technique also establishes a means for industry to *in situ* monitor the LZT process and other laser materials surface treatment applications.

## II. EXPERIMENTAL PROCEDURES

A Nd:YLF laser ( $\lambda = 1,047$  nm, full width at half maximum (FWHM)=15 ns) is used as the heating beam. The beam is expanded, attenuated, and focused onto the Ni–P sample (12 wt % of P) with a focal diameter of approximately 17.2  $\mu\text{m}$  measured using knife-edge profiling. The pulse energy is adjusted to create bumps with similar sizes and shapes to those used in the disk industry.

The novel PTD setup developed by Chen *et al.*<sup>10</sup> has been applied here to study the transient surface deformation of Ni–P disk substrates upon pulsed laser heating. In this setup, the probe He–Ne beam ( $\lambda = 632.8$  nm) is incident normal to the sample surface and collinear with the heating beam. The two beams form spots on the sample surface that are separated by approximately 2  $\mu\text{m}$ . When a single pulse with certain energy is fired onto the surface, the surface is deformed, causing deflection of the reflected He–Ne beam.

<sup>a)</sup>Electronic mail: cgrigoro@me.berkeley.edu

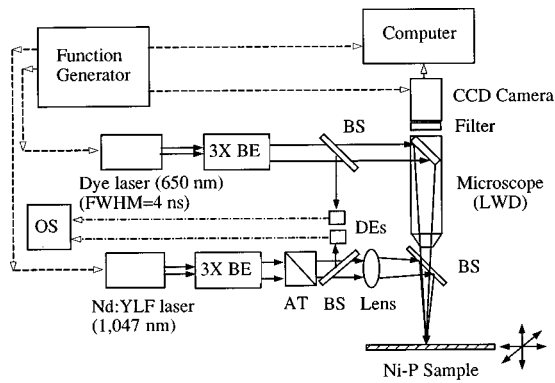


FIG. 1. Experimental setup of the laser flash photography system (AT: attenuator, BE: beam expander, BS: beam splitter, DE: Detector, OS: oscilloscope, LWD: long-working distance).

By detecting the deflection signal of the probe He–Ne beam, the transient deformation of the surface can be tracked with nanosecond-time-resolution.

In order to visualize the dynamic process of bump growth, a new LFP system is developed as shown in Fig. 1. A pulsed nitrogen laser-pumped dye laser ( $\lambda = 650 \text{ nm}$ ,  $\text{FWHM} = 4 \text{ ns}$ ) illuminates the sample surface through a long-working distance objective lens. The time-resolved images are obtained by synchronizing the laser flash with respect to the heating pulse. Each image frame contains information integrated over the laser-flash exposure period. It is noted that the technique can produce only a single image for each firing of the heating laser pulse. The image sequences are obtained by repeating the experiment under the same conditions based on the fact that the pulse-to-pulse instability of the heating laser is small, and the sample is uniform, thus yielding highly reproducible laser texture. Both the Nd:YLF laser and the dye laser are externally triggered by a pulse generator. The time interval between the two lasers is varied by the pulse generator and accurately measured by two fast photodiodes connected to an oscilloscope. This is to eliminate the delay variation due to possible jitter of the laser pulses. The spatial resolution of the imaging system is about  $1.0 \mu\text{m}$ , limited by the microscope magnification and the charge coupled device camera pixel size. The time resolution is within several nanoseconds, limited mainly by the dye laser pulse width.

### III. RESULTS AND DISCUSSION

The dependence of the bump shape (cross section) on the incident energy of the infrared heating beam is shown in Fig. 2 measured by atomic force microscopy (AFM). When the incident heating beam energy is  $4.0 \mu\text{J}$ , the bump has a crater at the center and a low peripheral rim, while the bump attains a ‘‘Sombrero’’ shape when the laser energy is  $2.0 \mu\text{J}$ . Integration of these profiles along a cross diameter indicates no net volumetric change, suggesting that material loss by ablation is minimal. The diameter of the bumps is about  $17 \mu\text{m}$  and the bump height varies from 50 to 10 nm. This change of the bump shape due to laser energy variation can be precisely identified in the probing beam deflection signals shown in Fig. 3. At heating beam energies exceeding  $2.7 \mu\text{J}$ ,

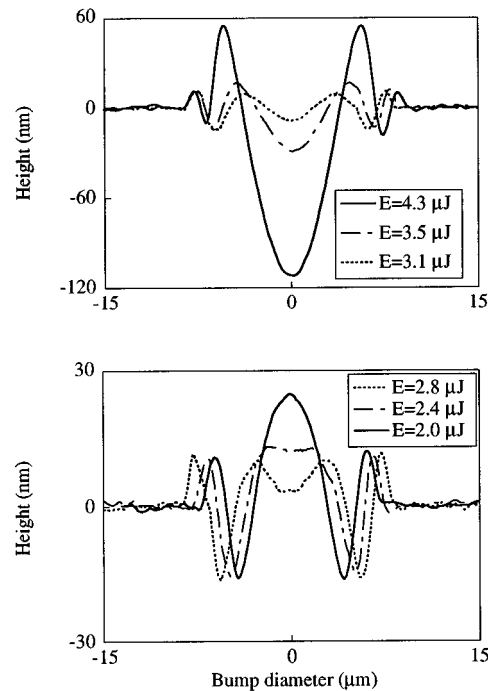


FIG. 2. Bump shape (cross section, measured by AFM) variation due to the incident heating beam energy change.

the deflection signal is enhanced, indicating a crater feature. At lower heating beam energies, such as  $2.0 \mu\text{J}$  for the Sombrero case, the growth of center peak reverses the slope sign if the location of the scanning He–Ne beam is fixed. Therefore, the deflection signal is reversed.

Furthermore, the deflection signals reveal transient information on the surface deformation process. For example, at the heating laser pulse energy of  $4.0 \mu\text{J}$ , the deflection signal increases to a maximum value at approximately 130 ns after the heating laser pulse. It then decreases gradually to a permanent value at about 800 ns. This transient process indicates that a crater is formed after melting. The crater becomes deeper and deeper until 130 ns, causing an increase of the slope of the crater with a correspondingly increasing deflection signal. After that, the crater recovers somewhat, con-

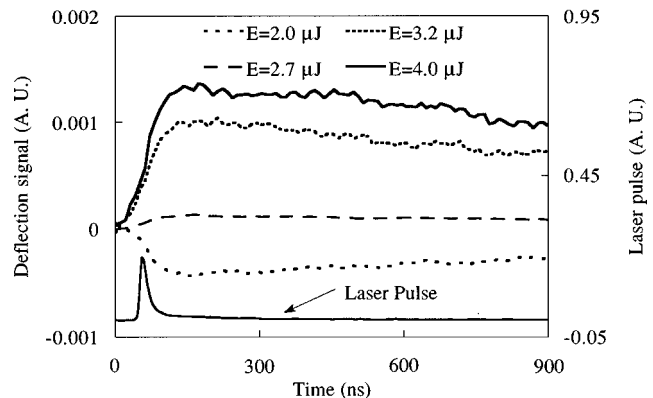


FIG. 3. Heating beam energy dependence of deflection signal. The deflection signal is enhanced due to the crater formation, and weakened for the Sombrero case.

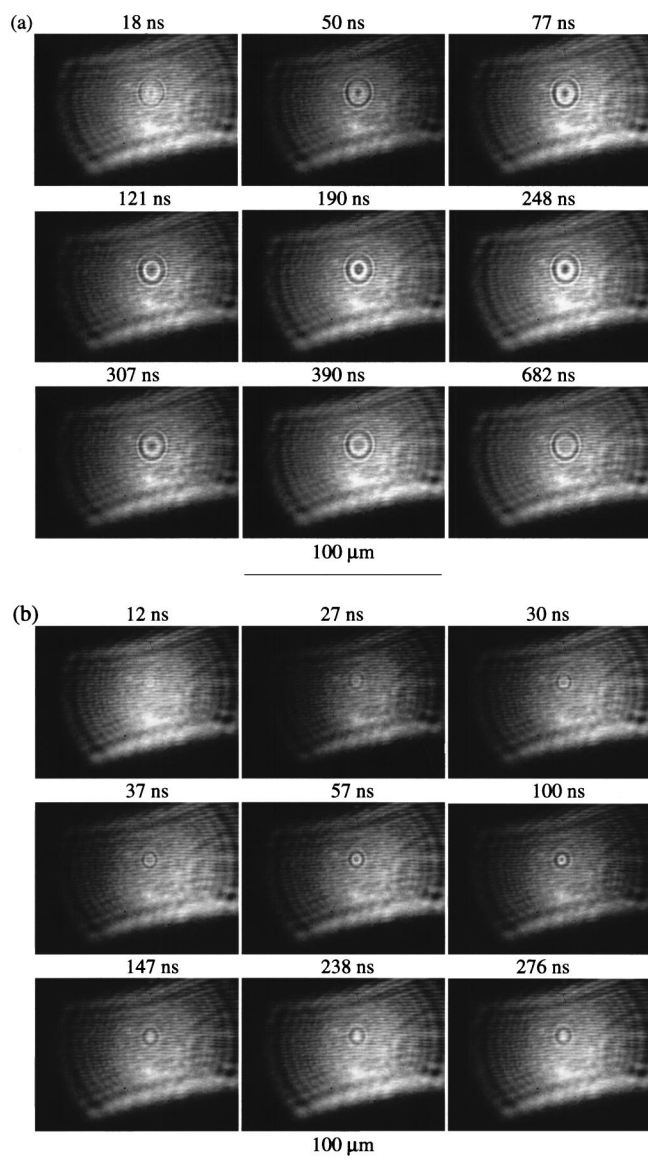


FIG. 4. A sequence of images of bumps with laser pulse energy of (a) 4.0  $\mu\text{J}$  and (b) 2.0  $\mu\text{J}$  produced by a laser flash photography system.

sequently the slope and deflection signal exhibit a small decrease until the surface is completely resolidified.

The visualization of the entire bump growth has been conducted for various pulse energies. As an example, Fig. 4(a) shows the sequence of images for the case with laser pulse energy equal to 4.0  $\mu\text{J}$ . A rim and a central hole become visible in the early stage, having formed right after melting. The melt pool expands and the hole diameter keeps increasing and deepening until 121 ns. It is in this period of time that the deflection signal in the photothermal displacement measurement increases and reaches a maximum value as discussed before. The photos from 121 to 682 ns show that there is some recovery at the central hole that causes the deflection signal reduction until the permanent state plateau. After 682 ns, no change is discernible and the solidification

process has concluded. This is also consistent with the results from the probe beam deflection detection and numerical simulation.<sup>5,14</sup> For the sombrero case, a similar sequence of images is shown in Fig. 4(b). A small and shallow depression is observed initially at the center of the growing protrusion. This “dimple” vanishes after about 100 ns, leaving the shiny central peak surrounded by a low-height peripheral rim, depicted in the micrograph as a faint halo. Since the probe beam diameter is about 5  $\mu\text{m}$  and positioned off-center, the deflection signal shown in Fig. 3 is dominated by the growth of the central peak.

Thermal emission contribution to the images has been examined by blocking the dye laser illumination. No significant thermal emission image can be captured even at the pulse energy of 6  $\mu\text{J}$ . Therefore, images in Fig. 4 are mainly due to the reflection of the dye laser beam.

#### IV. CONCLUSION

A new PTD scheme has been applied to diagnose the physical process of bump formation and a new nanosecond-time-resolution LFP is developed to visualize the bump growth dynamics in the LZT process of Ni–P hard disk substrates. The deflection signals show distinctly the variation of the produced surface features resulting from different pulse energies of the heating laser beam. Both the transient imaging and the transient deflection signals show consistently that the melted surface starts a partial recovery after the first hundred nanoseconds, and that the time scale of the surface motion is in the range of several hundred nanoseconds.

#### ACKNOWLEDGMENT

This work was conducted at the Laser Thermal Laboratory of the University of California at Berkeley.

- <sup>1</sup>R. Ranjan, D. N. Lambeth, M. Tromel, P. Goglia, and Y. Li, *J. Appl. Phys.* **69**, 5745 (1991).
- <sup>2</sup>D. Kuo *et al.*, *IEEE Trans. Magn.* **32**, 3753 (1996).
- <sup>3</sup>P. Baumgart, D. J. Krajnovich, T. A. Nguyen, and A. C. Tam, *IEEE Trans. Magn.* **31**, 2946 (1995).
- <sup>4</sup>A. C. Tam, I. K. Pour, T. A. Nguyen, D. J. Krajnovich, and P. Baumgart, *IEEE Trans. Magn.* **32**, 3771 (1996).
- <sup>5</sup>T. D. Bennett, D. J. Krajnovich, C. P. Grigoropoulos, P. Baumgart, and A. C. Tam, *J. Heat Transfer* **119**, 589 (1997).
- <sup>6</sup>H. K. Park, P. Kerstens, A. C. Tam, and P. Baumgart, *IEEE Trans. Magn.* **34**, 1807 (1998).
- <sup>7</sup>*Progress in Photoacoustic Science & Technology*, edited by A. Mandelis (Elsevier, New York, 1992), Vol. 1.
- <sup>8</sup>J. Opsal, A. Rosencwaig, and D. L. Willenborg, *Appl. Opt.* **22**, 3169 (1983).
- <sup>9</sup>M. A. Olmstead, N. M. Amer, S. Kohn, D. Fournier, and A. C. Boccara, *Appl. Phys. A: Solids Surf.* **32**, 141 (1983).
- <sup>10</sup>S. Chen, C. P. Grigoropoulos, H. K. Park, P. Kerstens, and A. C. Tam, *Appl. Phys. Lett.* **73**, 2093 (1998).
- <sup>11</sup>S. L. Jacques, G. Gofstein, and R. S. Dingus, *Proc. SPIE* **1646**, 284 (1992).
- <sup>12</sup>D. Kim and C. P. Grigoropoulos, *Appl. Surf. Sci.* **127–129**, 53 (1998).
- <sup>13</sup>J. Jandeleit, P. Rubbuldt, G. Urbasch, H. D. Hoffmann, H.-G. Treusch, E. W. Kreutz, *Proc. ICALEO'96 LIA* **81E**, 83 (1997).
- <sup>14</sup>M. Iwamoto, M. Ye, C. P. Grigoropoulos, and R. Greif, *Numer. Heat Transfer* (to be published).